

Article

Investigation of Alumina-Doped *Prunus domestica* Gum Grafted Polyaniline Epoxy Resin for Corrosion Protection Coatings for Mild Steel and Stainless Steel

Muhammad Kamran ¹, Anwar ul Haq Ali Shah ^{1,*}, Gul Rahman ¹, Salma Bilal ² and Philipp Röse ^{3,*}¹ Institute of Chemical Sciences, University of Peshawar, Peshawar 25120, Khyber Pakhtunkhwa, Pakistan² National Centre of Excellence in Physical Chemistry, University of Peshawar, Peshawar 25120, Khyber Pakhtunkhwa, Pakistan³ Karlsruhe Institute of Technology (KIT), Institute for Applied Materials-Electrochemical Technologies (IAM-ET), 76131 Karlsruhe, Germany

* Correspondence: anwarulhaqalishah@uop.edu.pk (A.u.H.A.S.); philipp.roese@kit.edu (P.R.)

Abstract: Eco-friendly inhibitors have attracted considerable interest due to the increasing environmental issues caused by the extensive use of hazardous corrosion inhibitors. In this paper, environmentally friendly PDG-g-PANI/Al₂O₃ composites were prepared by a low-cost inverse emulsion polymerization for corrosion inhibition of mild steel (MS) and stainless steel (SS). The PDG-g-PANI/Al₂O₃ composites were characterized by different techniques such as X-ray diffraction (XRD), UV/Vis, and FTIR spectroscopy. XRD measurements show that the PDG-g-PANI/Al₂O₃ composite is mostly amorphous and scanning electron micrographs (SEM) reveal a uniform distribution of Al₂O₃ on the surface of the PDG-g-PANI matrix. The composite was applied as a corrosion inhibitor on mild steel (MS) and stainless steel (SS), and its efficiency was investigated by potentiodynamic polarization measurement in a 3.5% NaCl and 1 M H₂SO₄ solution. Corrosion kinetic parameters obtained from Tafel evaluation show that the PDG-g-PANI/Al₂O₃ composites protect the surface of MS and SS with inhibition efficiencies of 92.3% and 51.9% in 3.5% NaCl solution, which is notably higher than those obtained with untreated epoxy resin (89.3% and 99.5%). In particular, the mixture of epoxy/PDG-g-PANI/Al₂O₃ shows the best performance with an inhibition efficiency up to 99.9% on MS and SS. An equivalent good inhibition efficiency was obtained for the composite for 1M H₂SO₄. Analysis of activation energy, formation enthalpy, and entropy values suggest that the epoxy/PDG-g-PANI/Al₂O₃ coating is thermodynamically favorable for corrosion protection of MS and exhibits long-lasting stability.

Keywords: PANI composite; corrosion protection; mild steel; Tafel analysis; epoxy resin; PDG; Al₂O₃; corrosion inhibition efficiency



Citation: Kamran, M.; Shah, A.u.H.A.; Rahman, G.; Bilal, S.; Röse, P. Investigation of Alumina-Doped *Prunus domestica* Gum Grafted Polyaniline Epoxy Resin for Corrosion Protection Coatings for Mild Steel and Stainless Steel. *Polymers* **2022**, *14*, 5128. <https://doi.org/10.3390/polym14235128>

Academic Editors: Valentina Sabatini and Daniela Meroni

Received: 24 October 2022

Accepted: 22 November 2022

Published: 25 November 2022

Publisher's Note: MDPI stays neutral with regard to jurisdictional claims in published maps and institutional affiliations.



Copyright: © 2022 by the authors. Licensee MDPI, Basel, Switzerland. This article is an open access article distributed under the terms and conditions of the Creative Commons Attribution (CC BY) license (<https://creativecommons.org/licenses/by/4.0/>).

1. Introduction

Many metals and steels are very susceptible to corrosion. As a result, huge quantities of metals are scrapped every year, causing enormous losses to the global economy. Protecting metals from corrosion is therefore essential to mitigate the limitations in industrial use. In this context, organic coatings have attracted much attention due to their excellent low-cost production, improved corrosion inhibition, excellent mechanical properties, high functionality, and environmental friendliness [1]. Among organic coatings, resins are widely used, especially water-based epoxy resins, which are applied for anti-corrosion coatings due to their excellent adhesion, corrosion-inhibiting properties, and mechanical durability [2]. Mechanical damage in organic coatings such as age-related brittleness, fractures, and external mechanical stress can compromise the integrity of the coating and reduce its long-term usability. The damage is difficult to detect and repair, and thus provides opportunities for oxygen and water to penetrate through cracks and cause

corrosion [3]. The development of self-healing coatings is key to repairing damaged surfaces spontaneously and thus protecting metal surfaces [4–10]. Currently, two types of self-healing coatings are used: First, coatings in which self-healing is achieved by reversible formation of hydrogen bonds with other functional groups. Second, coatings in which external components, such as hollow fibers or microcapsules containing repair agents, are incorporated into the coating. Once the coating is damaged, these repair agents are released to fill and repair the cracks, initiating self-healing [11–13]. Tao et al. developed a very efficient coating by adding silica nanoparticles (SNPs) and microcapsules to an aqueous epoxy resin. The corrosion current density was greatly affected by an increase or decrease in microcapsules and SNPs [8]. Ma et al. reported on epoxy resin coatings containing double-walled microcapsules to achieve self-healing ability with great success [14]. However, due to its high rigidity, low shock resistance, and hygroscopic properties, the use of epoxy resin as an anticorrosion coating has become questionable. The disadvantages can be compensated by using composites of different materials [15].

Nowadays, conductive polymers have multiple applications such as in energy storage, wastewater purification [16], sensing, and adsorption [17] and corrosion protection [18]. Among them, polyaniline (PANI) is widely used as a corrosion protection material due to its excellent physicochemical properties such as easy synthesis, redox reversibility, and good environmental compatibility [18]. Therefore, the incorporation of PANI into epoxy coatings has proven to be an excellent coating material for the corrosion protection of steel parts [19]. However, the environmental benefits of PANI, such as the introduction of materials from plants with excellent insulating and mechanical properties, have been little explored. These green materials are natural gums used alone or in combination with conductive polymers and metal oxides as coating materials for the corrosion protection of metals [20]. Natural gums are usually carbohydrates with electron-rich hydroxy functional groups that assist adhesion by forming a covalent bond with metal surfaces, thus forming an insulating layer, and reducing corrosion [21,22]. On the other hand, metal/metal oxide nanoparticles are added to the epoxy coating to increase the durability in harsh corrosive environments. Various metal oxides such as Fe_2O_3 , ZnO , TiO_2 , and ZrO_2 are commonly used in epoxy coatings to improve their corrosion protection [23].

In this paper, we report on the synthesis of PDG-g-PANI/ Al_2O_3 composite structures and their application in a corrosion protection system consisting of epoxy/PDG-g-PANI/ Al_2O_3 , which meets the requirements for an optimal and sustainable coating as a corrosion protection coating for stainless steel and MS in saline and acidic environment. Epoxy resin provides strong adhesion to the metal surface, high tensile strength, excellent insulation performance, and high thermal stability of the coating. PDG in the composite improved the insulating, anti-corrosive, and mechanical properties of a green approach to PANI. The introduction of Al_2O_3 into the polymer blend fills pores caused by the evaporation of the organic solvents during the drying process. Likewise, as a result, the composite possesses self-healing properties, which allow it to be used under highly corrosive conditions. Thus, the resulting epoxy/PDG-g-PANI/ Al_2O_3 coating showed promising corrosion protection properties for MS and SS in acidic and saline media.

2. Materials and Methods

2.1. Materials

Aniline ($\text{C}_6\text{H}_5\text{NH}_2$, Sigma Aldrich) was distilled two times under reduced pressure and was stored at low temperature prior to use. *Prunus domestica* gum (PDG) was collected from local gardens of district Peshawar, Pakistan, washed with distilled water, and was dried at room temperature for 14 days. The dried PDG was crushed and grinded to powder form. Diesel was purchased from Pakistan state oil (PSO, Karachi, Pakistan), with a boiling range from 160 to 366 °C, specific gravity of 0.828, and viscosity and 3.11 cst at 20 °C, respectively, and was used as received. Aluminum oxide (Al_2O_3 , Merck), benzoyl peroxide ($\text{C}_{14}\text{H}_{10}\text{O}_4$, Merck), dodecylbenzenesulfonic acid ($\text{C}_{12}\text{H}_{25}\text{C}_6\text{H}_4\text{SO}_3\text{H}$, DBSA, Acros organic), chloroform, *n*-hexane, methanol, ethanol, propanol, 2-butanol, acetone,

and *N*-methyl-2-pyrrolidone (NMP) were purchased from (Sigma Aldrich, St. Louis, MI, USA). Magic[®] epoxy glue (resin 100 g, hardener 80 g, 7 Mart Ltd., Punjab, Pakistan) with a mean viscosity of 16.500 cps and mean specific gravity of 1.10 was used without further treatment. Doubled distilled water was used for all the experiments.

2.2. Synthesis of PDG Grafted Polyaniline/Aluminium Oxide (PDG-g-PANI)/Al₂O₃ Composites

For the synthesis of the (PDG-g-PANI)/Al₂O₃ composite, 30 mL of distilled water was placed in a flask and then 0.1 g of Al₂O₃ powder was added and dispersed by ultrasonication for 30 min. Then, 0.1 g PDG powder was added under constant stirring. After 30 min, 1 mL of DBSA, 30 mL diesel and 0.4 mL of aniline were added to the suspension. For initializing polymerization, 1 g of BPO oxidant was added and the whole mixture was stirred at room temperature for 24 h. Over this time, a dark green product was precipitated. The product was washed with distilled water several times to remove water soluble impurities; a proper amount of acetone was added to disperse the product. The dispersion was poured into a ceramic tray and dried at room temperature. After drying, the product was washed with *n*-hexane for the removal of non-polar impurities. The obtained product was dried at 40 °C for 2 h.

2.3. Composite Characterisation Methods

UV/Vis spectra of PDG-g-PANI/Al₂O₃ were collected in chloroform in a spectral range from 200 to 1100 nm with a Lambda 1050 spectrometer (Waltham, MA, USA). Fourier transformed infrared spectroscopy (FTIR) was performed on an Affinity-1S FT-IR spectrometer from Shimadzu (Kyoto, Japan), scanning over an effective range of 400 to 4000 cm⁻¹, with a 2 cm⁻¹ resolution. X-ray diffraction (XRD) analysis was carried out using an X-ray diffractometer from Rigaku (Tokyo, Japan) with Cu K α radiation ($\lambda = 1.54 \text{ \AA}$) at 40 kV and 35 mA current with 2θ ranging from 10° to 80°, step width of 0.0164°, and a step rate of 1 s⁻¹. Imaging and structural analysis of the composites were performed using a scanning electron microscope (JSM-5910, JEOL, Tokyo, Japan).

2.4. Preparation of the Anti-Corrosion Coatings

Epoxy resin and hardener (1:1 *v/v*, total 0.5 g) were thoroughly mixed and applied together. Then PDG-g-PANI/Al₂O₃ (4.5 wt%) was suspended in 5 mL chloroform and mixed with the epoxy adhesive. The mixture was kept at room temperature for 30 min. Steel electrodes were polished using different sized sandpapers with 120 to 800 grit sizes and smoothed with a polishing pad containing alumina oxide suspension (0.05 μm), followed by washing with acetone, and double distilled water. Then the mixture 1 mL of the solution was drop casted on the MS or SS surface and dried at room temperature in an open atmosphere.

2.5. Electrochemical Characterization

Electrochemical characterizations of PDG-g-PANI/Al₂O₃ samples were carried out by using Reference 600 ZRA potentiostat/galvanostat (Gamry, Warminster, PA, USA), in three electrode assembly and in 1 M H₂SO₄ solution using gold sheet as the working electrode, gold wire as the counter, and saturated calomel electrode as the reference electrode. Cyclic voltammetry measurements were performed in the potential range -0.2 to 0.9 V at scan rates ranging from 10 mV s^{-1} to 500 mV s^{-1} .

Anti-corrosion analysis of the composite was performed in a corrosive solution of 3.5% NaCl and 1M H₂SO₄. Corrosion experiments for blank and coated MS and SS disks were performed in a customized cell with three electrodes using the Reference 600 ZRA potentiostat/galvanostat (Gamry, Warminster, PA, USA). MS and SS disks were used as the working electrodes, saturated calomel electrodes (SCE) as the reference electrodes, and stainless-steel plates as the counter electrodes. Cathodic/anodic potentiodynamic polarization measurements were performed and corrosion kinetic parameters such as i_{corr} (corrosion current density), E_{corr} (corrosion potential) and the corrosion rate C_{R} (mm/year)

for MS and SS were calculated by extrapolating Tafel plots using Gamry Echem Analyst software. The inhibition efficiency was determined by using Equation (1).

$$\text{Inhibition efficiency (I.E.)\%} = 1 - \frac{i_{corr}}{i_{corr}^0} \times 100 \quad (1)$$

where i_{corr}^0 is the corrosion current density of blank steel electrodes, while i_{corr} is the corrosion current density of coated steel electrodes.

The corrosion rate was calculated using the weight loss per time. To ensure an accurate measurement, two comparable electrodes were polished, then thoroughly cleaned with ethanol, acetone, and distilled water, dried in an oven to constant weight and weighed. Then, one of the electrodes was coated with the composite and tested for corrosion resistance under saline and acidic conditions. An uncoated electrode was used as a reference sample. The corrosion rate was then calculated according to Equation (2):

$$\text{Corrosion rate} = \frac{W}{D \cdot A \cdot t} \quad (2)$$

where W is weight loss in g, D is density in g cm^{-3} , A is area in cm^2 , and t is time of exposure in seconds (s).

3. Results and Discussion

3.1. Solubility Study

The composite solubility is an important property from an application point of view since both the processability and the resistance in different areas of the application are key criteria. To investigate the solubility of the PDG-g-PANI/ Al_2O_3 composite, various organic solvents were explored (Figure 1). It was found that the composite is soluble in alcohols, especially methanol and ethanol/propanol, which is due to the presence of polar components such as $-\text{NH}$ and $-\text{OH}$, which are responsible for the solubility in polar solvents. Such solubility can be attributed to the formation of hydrogen bonds between composites and alcohols [20]. The same phenomenon occurred when the composite approached NMP and THF, albeit these solvents differ significantly from alcohols. The presence of the amide and ether functional groups in NMP as well THF may form hydrogen bonds with $-\text{OH}$ of PDG and $-\text{NH}$ of PANI in the composite particles.

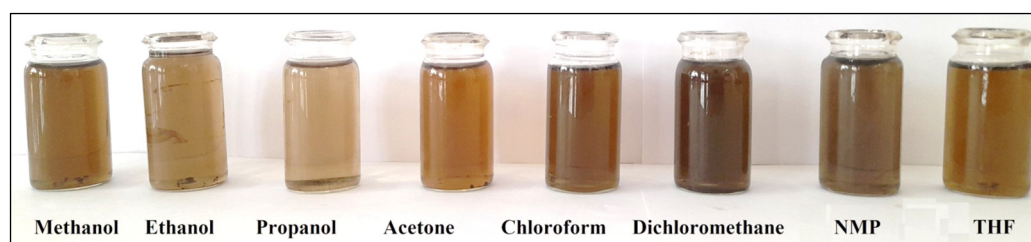


Figure 1. Solutions of PDG-g-PANI/ Al_2O_3 in various common organic solvents.

The solubility of the composite in dichloromethane can be attributed to a dipole-dipole interaction, since the composite is doped with DBSA, which contains both a nonpolar alkyl chain and a polar sulfonate group. The solubility of the composite in nonpolar solvents such as acetone and chloroform are due to the nonpolar interaction between the solvent and the nonpolar components present in the composite [24,25].

3.2. UV/Visible Spectroscopy

The absorption spectra of neat PDG and PANI, PDG-g-PANI, and PDG-g-PANI/ Al_2O_3 in chloroform were recorded by UV/Vis (200–1100 nm, see Figure 2). The arbinogalactan components of PDG showed absorption at 272 nm. The spectrum of PANI revealed peaks at 276 nm, 402 nm, and a broadened characteristic at 600 nm. These peaks were due to the

π - π^* -transition of the benzoid ring, the polaron π^* -transition of the quinoid ring, and the π -polaron transition [26]. The PDG-g PANI spectrum exhibited peaks at 259 nm, 301 nm, 407 nm, and a broadened feature at 556 nm. The region at 556 nm is attributed to the π -polaron transition, while the peak at 407 nm is attributed to the polaron π^* -transition of the quinoid ring. Peaks at 301 nm and 261 nm are attributed to the π - π^* -transition of the benzoid ring and the arabinogalactose component of PDG, respectively [20]. The UV/Vis spectra of PDG-g-PANI/ Al_2O_3 gave three sharp peaks at 251 nm, 290 nm, and 403 nm, while there was one broad peak at 573 nm. The occurrence of sharp peaks is due to the incorporation of Al_2O_3 into the PDG-g-PANI backbone. The peak at about 251 nm is attributed to the arbinogalactan components of PDG, while the sharp peak at 290 nm originates from the benzoid ring of PANI. A clear blue shift is observed in both peaks, which can be attributed to the incorporation of Al_2O_3 into the polymer chain. The peak at about 407 nm is attributed to the polaron- π^* transition of the quinoid ring, while a broad absorption peak at 573 nm is attributed to the exciton transition in the composite. All these peaks indicate the formation of PDG-g-PANI/ Al_2O_3 .

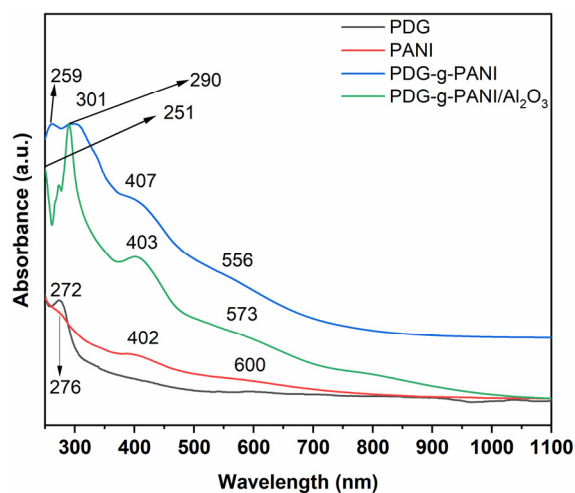


Figure 2. UV/Vis spectra of PDG, PANI, PDG-g-PANI, and PDG-g-PANI/ Al_2O_3 .

3.3. FTIR Analysis

Figure 3 shows the FTIR spectra of PDG, PANI, PDG-g-PANI, and PDG-g-PANI/ Al_2O_3 , and the peak assignments concerned are given in Table 1 [20]. In the spectrum of PDG-g-PANI/ Al_2O_3 , the bands at 2917 cm^{-1} and 2847 cm^{-1} are due to coupled stretching vibrations of the aliphatic C-H of PDG and C-H of aniline in the polymer chain. The typical peak of -COOH occurring at 1716 cm^{-1} due to the stretching vibration of -C=O confirms the grafting of PDG into the polymer chain. The peak at 1490 cm^{-1} and 1451 cm^{-1} is assigned to the C=C stretching of quinolines and benzene rings, respectively [27]. The shift in quinoid stretching indicates the doping of the polymer chain with metal oxide. The peak at 1372 cm^{-1} is due to C-N stretching, while the peak at about 1003 cm^{-1} is assigned to C-H stretching vibration. The peak at 826 cm^{-1} was due to out-of-plane C-H deformation. The band at 753 cm^{-1} is assigned to the C-H bending vibration, while the occurrence of the peak at 1003 cm^{-1} is due to -SO₃H of DBSA, confirming the doping of DBSA into the polymer chain [26]. The peak at 689 and 580 cm^{-1} is attributed to Al_2O_3 , confirming the incorporation of Al_2O_3 into the PDG-g-PANI chain [28].

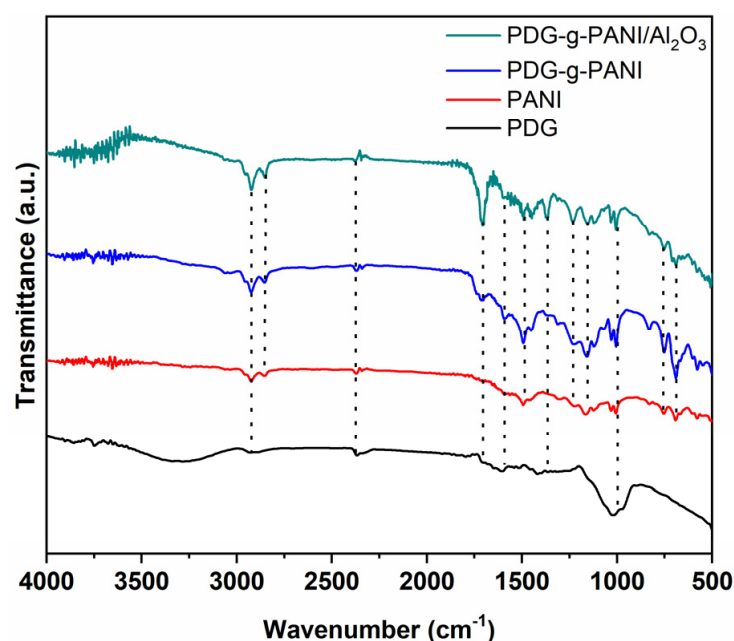


Figure 3. FTIR spectra of the PDG, PANI, PDG-g-PANI, and PDG-g-PANI/Al₂O₃.

Table 1. FTIR peak position and its assignment of PDG, PANI, PDG-g-PANI, and PDG-g-PANI/Al₂O₃.

PDG	Peak Assignment	PANI	Peak Assignment	PDG-g-PANI	Peak Assignment	PDG-g-PANI/Al ₂ O ₃	Peak Assignment
3291	–OH	3241	ν NH ₂	/		/	
2915	ν aliphatic C–H	2930	ν C–H of aniline ring	2921	ν C–H of aniline ring	2917	ν C–H of aniline ring
/		2851		2851		2847	
2363		2369		2370		/	
1791	ν C=O of –COOH	/		1716	ν C = O of –COOH	1716	ν C = O of –COOH
1605	ν conjugated C=C	/		/		/	
1509		1583	ν C–N of Quinoid ring	1593	ν Quinoid ring C–N	1490	ν Quinoid ring C–N
1413		1489	Benzenoid ring	1498	Benzenoid ring	1451	Benzenoid ring
/	ν C–O	1303	C–N	1314	ν C–N	1372	ν C–N & δ C–H
/		1170	δ C–H	1158	δ C–H	1003	–SO ₃ H of DBSA
1023	ν C–O bond	1008	–SO ₃ H of DBSA	1000	ν C–O bond	689	Al ₂ O ₃
/		573	SO ₃ ^{–1} of DBSA	573	SO ₃ ^{–1} of DBSA	580	Al ₂ O ₃

3.4. X-ray Diffraction

The XRD pattern of pristine Al₂O₃, PDG, PDG-g-PANI, and PDG-g-PANI/Al₂O₃ is shown in Figure 4. The XRD pattern of Al₂O₃ exhibits characteristic diffraction peaks at 37.5°, 45.7°, 66.6° corresponding to (311), (400), and (440) lattice planes of γ -Al₂O₃ [29]. Both the pristine PDG and the PDG-g-PANI show broad peaks in the range of 17° and 21°, indicating the amorphous nature of the natural rubber and the polymer. The incorporation of Al₂O₃ in the PDG-g-PANI matrix as a nanofiller did not change the mainly amorphous structure [30].

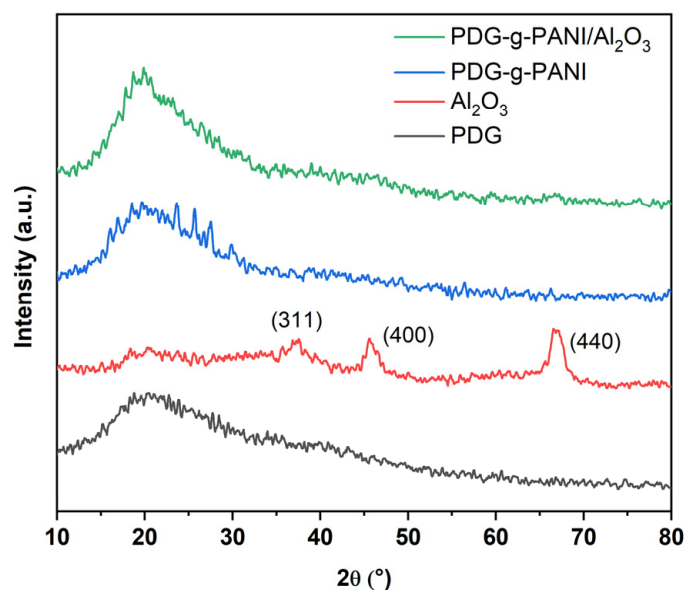


Figure 4. XRD pattern of pristine Al_2O_3 , PDG, PDG-g-PANI, and PDG-g-PANI/ Al_2O_3 .

3.5. Energy Dispersive X-ray Analysis

Energy dispersive X-ray (EDX) analysis was performed to verify the incorporation of Al_2O_3 into the PDG-g-PANI matrix. The result is shown in Figure 5, and the corresponding elemental composition is listed in Table 2. The high carbon content originates from aniline and PDG in the composite, since it is the main content in both compounds. The sulfur content of 4.65 wt% indicates an efficient doping of the PANI backbone by DBSA, while the presence of alumina confirms the incorporation of Al_2O_3 into the polymer matrix.

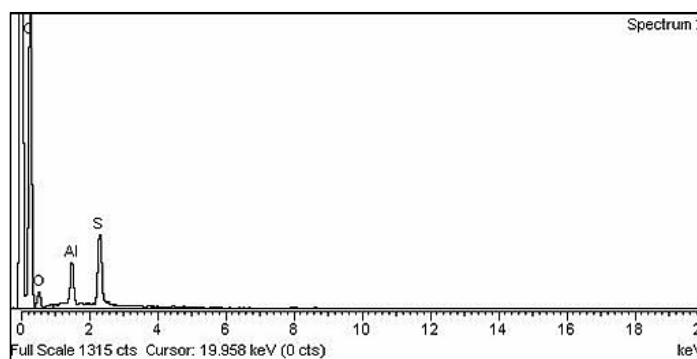


Figure 5. EDX spectrum of PDG-g-PANI/ Al_2O_3 .

Table 2. EDX data showing the percentage composition of PDG-g-PANI/ Al_2O_3 .

Element	Weight (%)	Atomic (%)
C	81.99	88.07
O	11.19	9.03
S	2.16	1.03
Al	4.65	1.87
Total	100	100

3.6. Scanning Electron Microscopy Analysis

SEM images of PDG, PANI, PDG-g-PANI, and PDG-g-PANI/ Al_2O_3 are shown in the Figure 6. PANI exhibits a porous morphology while the PDG shows irregular surface characteristics. The image of PDG-g-PANI displays a porous surface of PANI having a PDG

network surrounding the porous network of PANI [20]. For PDG-g-PANI/Al₂O₃ it can be seen that all three components including PANI, PDG, and Al₂O₃ particles are present in the composite. PANI forms the principal matrix surrounded by the fibrous network of PDG. It is noticed that Al₂O₃ particles are distributed along the whole network of the composite. The images show that PDG and alumina particles block the pores in the matrix of the polymer and thus restrict the movement of corrosive ions to reach the metal surface, protecting it from corrosion. This results in an increase in corrosion protection capability.

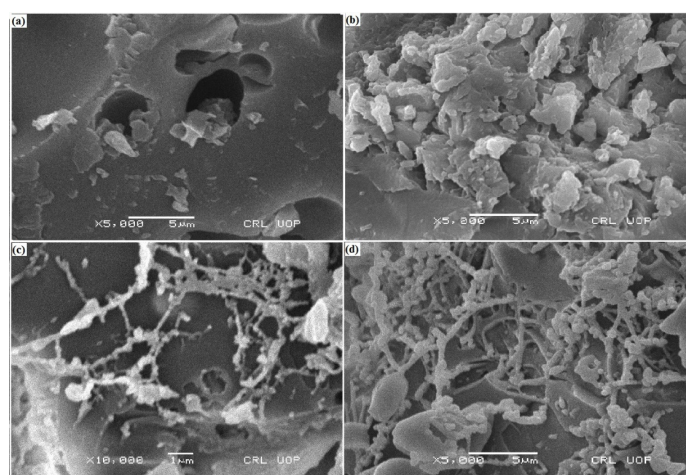


Figure 6. SEM micrographs of (a) PANI (b) PDG (c) PDG-g-PANI, and (d) PDG-g-PANI/Al₂O₃.

3.7. Cyclic Voltammetry

Figure 7 displays the cyclic voltammogram of PDG-g-PANI/Al₂O₃ at different scan rates from 10 to 90 mV s^{−1} obtained in 1 M aqueous H₂SO₄ solution in the potential range of −0.2 to 0.9 V. The CV exhibits the two characteristic oxidation and reduction peaks of PANI. The first peak at E_{SCE} = 0.19 V is assigned to the conversion of neutral leucoemeraldine to the partially oxidized emeraldine form of PANI, while the second oxidation peak at 0.60 V is attributed to the redox transition of the emeraldine to pernigraniline. In the reverse scan, the conversion of pernigraniline to emeraldine is at 0.68 V, while the peak at −5 mV shows the conversion of the emeraldine form of PANI back to the fully reduced leucoemeraldine [31]. The observed redox peaks are particularly associated with the PANI composite, indicating that the polymerization of aniline in the presence of PDG and Al₂O₃ nanoparticles generates an electroactive reversible composite.

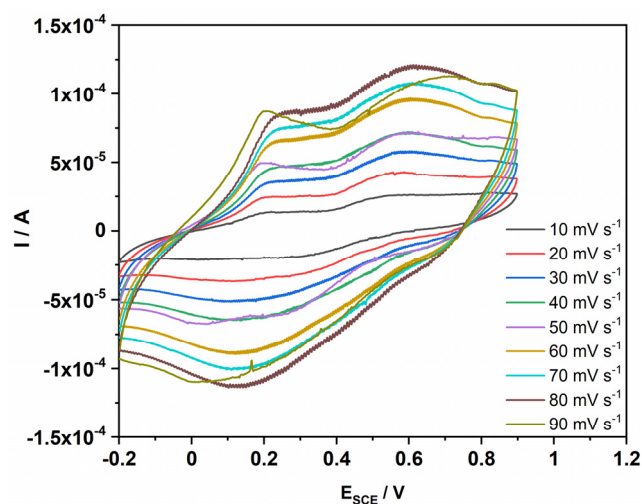


Figure 7. Cyclic voltammogram of PDG-g-PANI/Al₂O₃ at different scan rates obtained in 1 M aqueous H₂SO₄ solution.

3.8. Investigation of the Corrosion Behavior

3.8.1. Potentiodynamic Polarization Study of Mild Steel in NaCl Solution

Potentiodynamic polarization measurement is a suitable analysis technique for corrosion protection coating systems. Tafel curves of the uncoated, bare composite, bare epoxy, and epoxy/composite coated mild steel (MS) immersed in 3.5 wt% NaCl solution are shown in Figure 8. The corrosion kinetic parameters calculated from polarization curves by Tafel extrapolation are presented in Table 3. The corrosion current density and corrosion potential of uncoated MS are $20.2 \mu\text{A}$ and -777 mV , with a corrosion rate of 9.224 m/year . The PDG-g-PANI/ Al_2O_3 coating on MS reduces the current density to $1.56 \mu\text{A}$, thus shifting the corrosion potential to -420 mV and reducing the corrosion rate to 0.711 m/year with an inhibition efficiency of 92.3%. The pristine epoxy coating on MS also shows an inhibition efficiency of 89.3%. Incorporation of the PDG-g-PANI/ Al_2O_3 composite into the epoxy coating inhibits the surface of MS by two simultaneous effects: (1) the inorganic Al_2O_3 particles in polymer coating provides a physical barrier for the corrosive environment from reaching the metal surface by filling the nanopores and micropores in the coating [32,33]; (2) the PDG-g-PANI matrix enhances the corrosion protection of epoxy coating due to its electrical conductivity and the formation of a strong protective oxide layer on the MS surface [34]. The lowest current density and inhibition efficiency of 99.9% indicates that the presence of Al_2O_3 has a great impact on epoxy/composite coating.

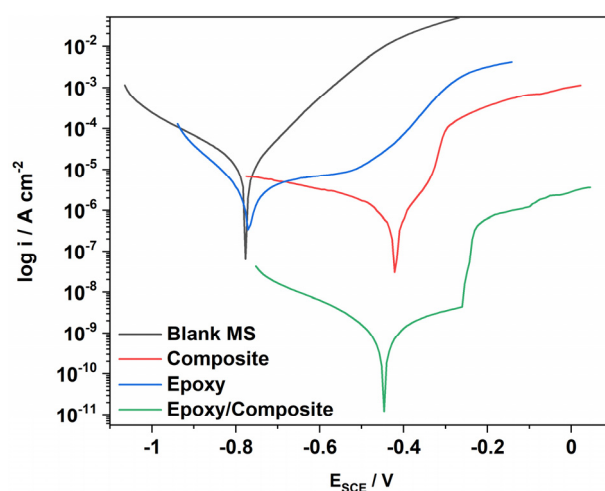


Figure 8. Tafel plot of uncoated, PDG-g-PANI/ Al_2O_3 , Epoxy, and Epoxy/PDG-g-PANI/ Al_2O_3 coated MS in 3.5% NaCl.

Table 3. Corrosion parameters of blank, PDG-g-PANI/ Al_2O_3 , Epoxy, and Epoxy/PDG-g-PANI/ Al_2O_3 coated MS in 3.5% NaCl calculated from the polarization curves by Tafel extrapolation.

Coating	β Anode (V/dec)	β Cath. (V/dec)	I_{corr} (μA)	E_{corr} (mV)	Corrosion Rate (m/Year)	Inhibition Efficiency (%)
Blank MS	0.140	0.207	20.2	-777	9.224	/
Epoxy	0.300	0.099	2.16	-768	0.988	89.3
PDG-g-PANI/ Al_2O_3	0.142	0.539	1.56	-420	0.711	92.3
Epoxy/composite	0.328	0.225	0.014	-447	0.00068	99.9

3.8.2. Corrosion Study of Stainless Steel in NaCl Solution

The behavior of uncoated and composite, epoxy and epoxy/composite coated SS were also tested in 3.5% NaCl solution and the results are shown in Figure 9 and Table 4. Uncoated SS shows a corrosion current density of $11.9 \mu\text{A}$ and -960 mV for the corrosion overpotential, with a corrosion rate of 5.42 m/year . With coating, the corrosion rate decreases to 2.616 m/year with a lowered corrosion current density of $5.72 \mu\text{A}$, a positive

shift of corrosion potential value of -563 mV, and an inhibition efficiency of 52%. However, the PDG-g-PANI anti-corrosion behavior is still moderate, which can be attributed to the low adhesion on SS, which allows the salt solution to penetrate the surface of the steel and cause corrosion. For improvement, the composite was integrated into an epoxy matrix with strong adhesion and mechanical durability. The epoxy/composite coating on SS shows an excellent anti-corrosion behavior with a corrosion rate of 0.0051 m/year and efficiency of 99.9%.

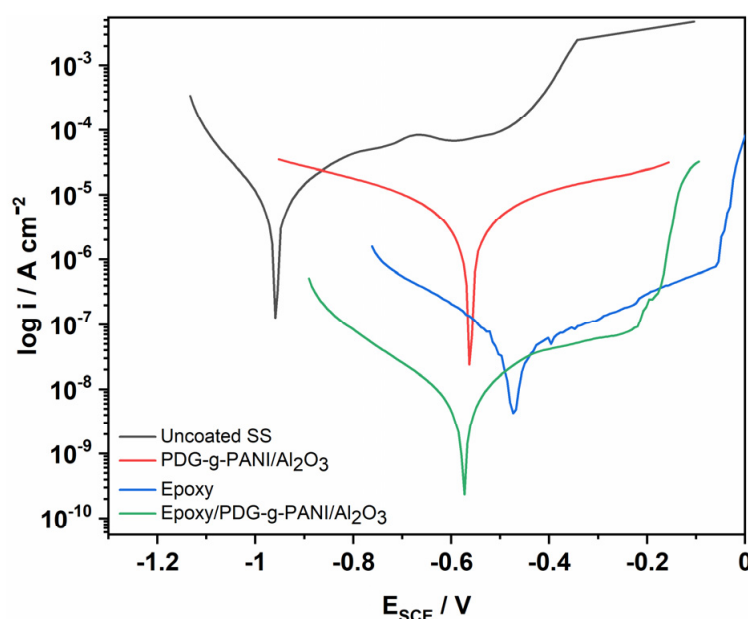


Figure 9. Tafel plot of uncoated, PDG-g-PANI/ Al_2O_3 , Epoxy, and Epoxy/PDG-g-PANI/ Al_2O_3 coated SS in 3.5% NaCl.

Table 4. Corrosion parameters of uncoated, PDG-g-PANI/ Al_2O_3 , Epoxy, and Epoxy/PDG-g-PANI/ Al_2O_3 coated SS in 3.5% NaCl calculated from polarization curves by Tafel extrapolation.

Coating	β Anode (V/dec)	β Cath. (V/dec)	I_{corr} (μA)	E_{corr} (mV)	Corrosion Rate (m/Year)	Inhibition Efficiency (%)
Blank SS	0.444	0.163	11.90	-960	5.421	/
Epoxy	0.351	0.206	0.055	-471	0.022	99.53
Composite coated	0.535	0.463	5.72	-563	2.616	51.93
Epoxy/composite coated	0.362	0.237	0.011	-584	0.0051	99.90

3.8.3. Potentiodynamic Polarization Study of Mild Steel in H_2SO_4 Solution

The corrosion protection ability of PDG-g-PANI/ Al_2O_3 , pristine epoxy, and the blend of epoxy with PDG-g-PANI/ Al_2O_3 on MS were investigated in 1 M H_2SO_4 and were compared with uncoated MS (Figure 10 and Table 5). The results of the corrosion current and corrosion potential for uncoated MS are $1480 \mu\text{A}$ and -508 mV. By coating PDG-g-PANI/ Al_2O_3 on MS, the corrosion current density decreases to $11.80 \mu\text{A}$ and E_{corr} is shifted to -475 mV, showing excellent corrosion protection with an inhibition efficiency of 99.2%. On the other hand, the coating of pristine epoxy on MS decreases the corrosion current to $2.05 \mu\text{A}$, displaying an inhibition efficiency of 99.86%. However, the coating of epoxy with composite coating inhibits the surface of steel tremendously from corrosion through the synergistic effect of all components present in a single coating. The coating reduces the corrosion current density to $0.473 \mu\text{A}$, which is almost 1.5 times lower than for the epoxy resin, revealing an enhanced corrosion protection with perfect inhibition

efficiency of 99.96% and corrosion rate of 0.216 m/year. The results conclude that PDG-g-PANI/Al₂O₃ blended with epoxy possesses excellent behavior as a corrosion inhibition coating in strongly acidic medium.

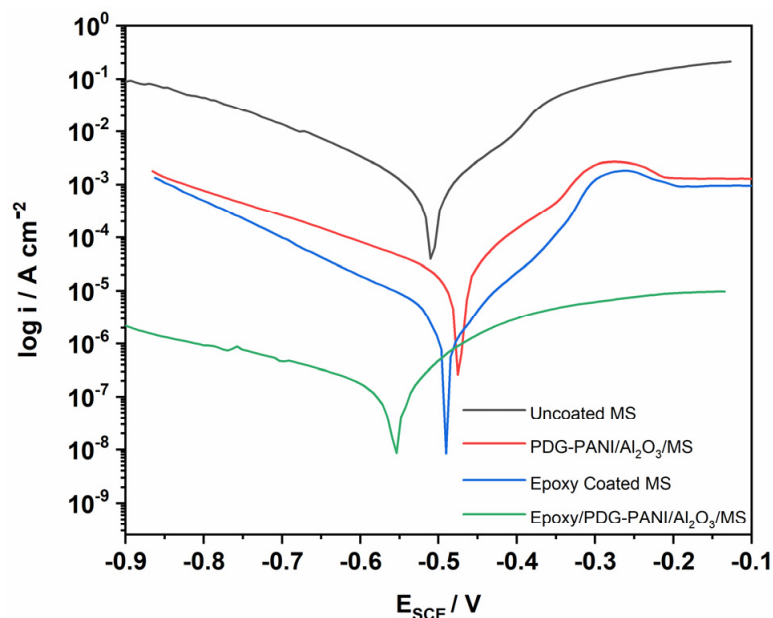


Figure 10. Tafel plot of uncoated, PDG-g-PANI/Al₂O₃, Epoxy, and Epoxy/PDG-g-PANI/Al₂O₃ coated MS in 1 M H₂SO₄.

Table 5. Corrosion parameters of uncoated, PDG-g-PANI/Al₂O₃, Epoxy, and Epoxy/PDG-g-PANI/Al₂O₃ coated SS in 1 M H₂SO₄ calculated from polarization curves by Tafel extrapolation.

Coating	β Anode (V/dec)	β Cath. (V/dec)	I_{corr} (μA)	E_{corr} (mV)	Corrosion Rate (m/Year)	Inhibition Efficiency (%)
Blank MS	0.159	0.209	1480	−508	675.3	/
Epoxy	0.079	0.128	2.05	−490	0.939	99.86
PDG-g-PANI/Al ₂ O ₃	0.079	0.175	11.8	−475	5.370	99.2
Epoxy/Composite	0.275	0.715	0.47	−556	0.216	99.96

3.8.4. Potentiodynamic Polarization Study of Stainless Steel in H₂SO₄ Solution

The corrosion behavior of stainless steel in H₂SO₄ solution is shown in the following (Figure 11 and Table 6). Firstly, blank SS was tested towards its corrosion properties. The corrosion rate is 2157 m/year with 4.72 mA corrosion current density and −491 mV corrosion potential. When coated with PDG-g-PANI/Al₂O₃ the corrosion current density decreases to 96.8 μA and shifts to a corrosion potential positively with −458 mV and a decrease in corrosion rate to 44.2 m/year (97.9% inhibition efficiency). By coating pristine epoxy resin the corrosion current density and voltage drop to 6.65 μA and −470 mV with 3.03 m/year corrosion rate and 99.85% inhibition efficiency. The combination of epoxy resin and composite result in an excellent corrosion rate of 0.014 m/year and 99.99% inhibition. The behavior of epoxy/composite coating on SS is attributed to the fact the combined epoxy/composite coating contains an optimal sticky epoxy resin with good mechanical strength, PDG with sticky behavior due to presence of electron rich functional groups and good mechanical properties, PANI with its redox reversible nature and Al₂O₃ with its mechanical barrier property, self-healing ability, and its resistivity [18].

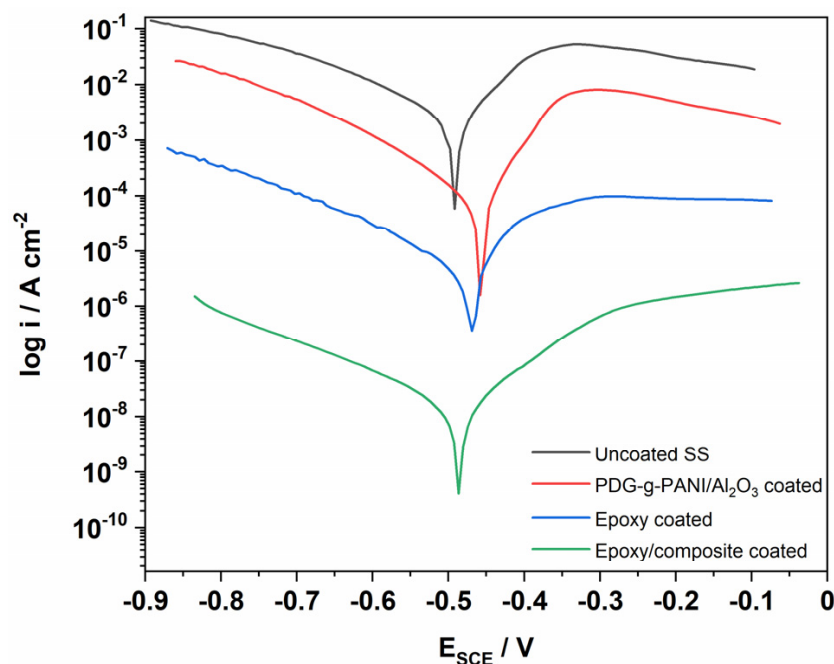


Figure 11. Tafel plot of uncoated, PDG-g-PANI/Al₂O₃, Epoxy, and Epoxy/PDG-g-PANI/Al₂O₃ coated SS in 1 M H₂SO₄.

Table 6. Corrosion parameters of uncoated, PDG-g-PANI/Al₂O₃, Epoxy, and Epoxy/PDG-g-PANI/Al₂O₃ coated SS in 1 M H₂SO₄ calculated from polarization curves by Tafel extrapolation.

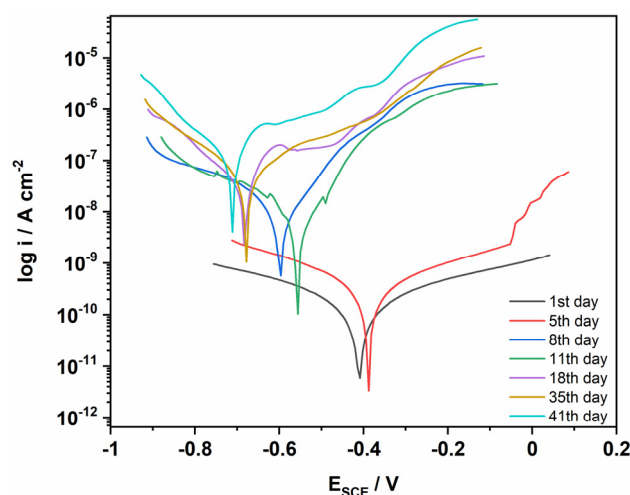
Coating	β Anode (V/dec)	β Cath. (V/dec)	I_{corr} (μA)	E_{corr} (mV)	Corrosion Rate (m/Year)	Inhibition Efficiency (%)
Blank SS	0.138	0.257	4720	−491	2157	/
Epoxy	0.131	0.193	6.65	−470	3.03	99.85
PDG-g-PANI/Al ₂ O ₃	0.073	0.152	96.8	−458	44.2	97.9
Epoxy/Composite	0.211	0.239	0.0318	−490	0.014	99.99

3.8.5. Kinetic Study in Real Outdoor Environment

The kinetic study of epoxy/composite coated MS was studied outdoors with constant treatment by salt spray after 24 h for 41 days at room temperature. The material was applied to the polished surface of the MS and dried at room temperature. After drying, the anti-corrosion behavior of the coating was tested using the potentiodynamic polarization technique in 3.5% NaCl solution. After that, the samples were stored outdoors and subjected to constant salt spray treatment every 24 h, and the corrosion ability of the coating was checked at constant time intervals. The corrosion kinetic parameters obtained from the Tafel extrapolation are shown in Table 7 and the Tafel plots are shown in Figure 12. The corrosion rate of the epoxy/composite coating decreased to a large extent after the first day of coating compared to uncoated MS. The behavior of the coating was observed at different time intervals, and it was found that the coating exhibited excellent anti-corrosion protection behavior to the surface of the MS for 41 days. After 41 days, the calculated inhibition efficiency was 99.3% with a corrosion rate of 0.0626 m/year, showing sufficient inhibition over a long period of time.

Table 7. The corrosion kinetic parameters of PDG-g-PANI/Al₂O₃ coated MS over 41 days.

Coating Duration	β Anode (V/dec)	β Cath. (V/dec)	I_{corr} (μA)	E_{corr} (mV)	Corrosion Rate (m/Year)
Blank MS	0.140	0.207	20.2	−777	9.224
1st day	0.721	0.703	20.2×10^{-6}	−407	0.00015
5th day	0.559	0.496	609×10^{-6}	−384	0.00028
8th day	0.150	0.307	16.2×10^{-3}	−594	0.0074
11th day	0.147	0.318	13.4×10^{-3}	−522	0.0061
18th day	0.218	0.152	35×10^{-3}	−681	0.0159
35th day	0.237	0.172	52×10^{-3}	−679	0.0239
41st day	0.230	0.148	137×10^{-3}	−713	0.0626

**Figure 12.** Tafel plots of Epoxy/PDG-g-PANI/Al₂O₃ coated MS under outdoor conditions.

3.8.6. Weight Losses during Corrosion

Quantification of the weight loss during the corrosion experiments were performed by immersing the uncoated and the epoxy/(PDG-g-PANI/Al₂O₃) coated MSs in a 3.5% NaCl solution for 25 days at room temperature. The corrosion rate was calculated for both the uncoated and coated electrodes based on the weight loss. The corresponding inhibition efficiencies were calculated from the corrosion rates for uncoated and coated MS; the results are shown in Table 8. The weight loss for uncoated MS was 129 mg after 25 days of immersion in 3.5% NaCl solution, whereas the weight loss of PDG-g-PANI-coated MS was 5 mg. According to the calculation, the corrosion rate of the uncoated MS was 2.41 m/year and that of the coated MS was 0.093 m/year with an inhibition efficiency of 96.1%. The results were in close agreement with the electrochemical data.

Table 8. Weight loss of uncoated and coated MS before and after immersion with the corresponding corrosion rate and inhibition efficiency.

Sample	Weight before Immersion (g)	Weight after Immersion (g)	Weight Loss (g)	Corrosion Rate (m/Year)	Inhibition Efficiency (%)
Blank MS	62.926	62.797	0.129	2.41	/
PDG-g-PANI	59.763	59.753	0.005	0.093	96.1

3.8.7. Analysis of the Temperature Dependency on the Corrosion Rate

For an in-depth explanation of the corrosion protection properties of the coating, the thermodynamic parameters such as activation energy, change in formation enthalpy and entropy were determined for uncoated and epoxy/PDG-g-PANI/Al₂O₃ coated MS. The effect of temperature on the anticorrosion reaction of the coating is complex and leads

to changes in the metal surface state by desorption of the inhibitor, rapid etching, and decomposition or restructuring of the coating material. Based on the potentiodynamic polarization curve, it was observed that the corrosion rates for both coated and uncoated MS in 3.5% NaCl solutions increase with the increasing temperature (Figure 13).

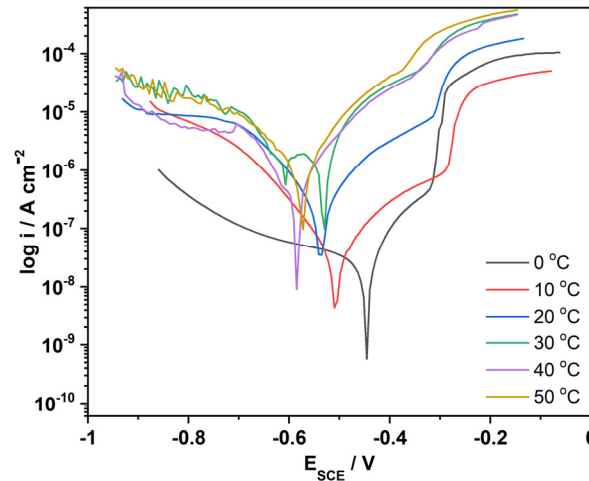


Figure 13. Tafel plot of Epoxy/composite coated MS at different temperatures.

It is well understood that the activation energy depends on temperature, which can be calculated from Arrhenius Equation (3). The logarithm of the corrosion rate C_r is plotted against $1/T$, as given below,

$$\log C_r = -\frac{E_a}{RT} + \ln A \tag{3}$$

where E_a is the activation energy, R is the universal gas constant, and T is the Kelvin temperature (Figure 14a,b). The E_a values are calculated from the slope of the graph and are given in Table 9. The activation energy for coated MS is higher than for uncoated MS in a 3.5% NaCl solution, indicating a strong inhibition behavior through the coating by reducing the reaction rate for the corrosion process. It confirms once more the strong adsorption of the epoxy/composite coating towards a mild steel surface, and thus a superficial anti-corrosion behavior [35].

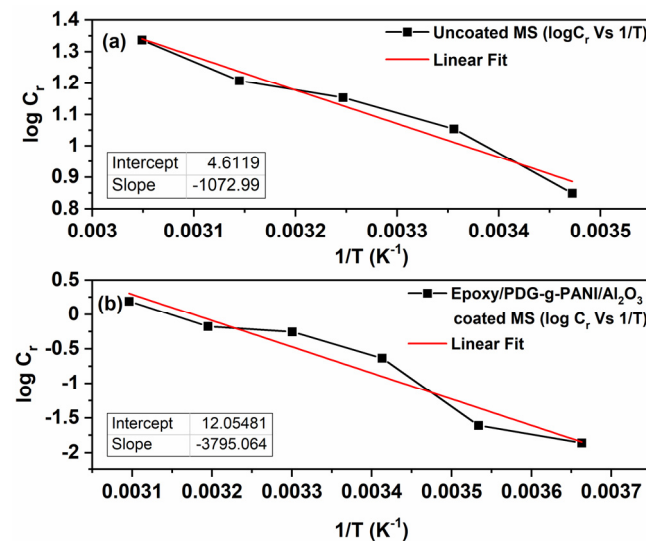


Figure 14. Arrhenius plots of $\log C_r$ versus $1/T$ for (a) uncoated MS and (b) Epoxy/composite coated MS.

Table 9. Calculated thermodynamic parameters including apparent activation energy, entropy change, and enthalpy change in 3.5% NaCl for uncoated and Epoxy/PDG-g-PANI/Al₂O₃ MS.

Sample	Activation Energy (E _a /kJ)	Enthalpy (ΔH/kJ mol ⁻¹)	Entropy (ΔS/kJ K ⁻¹)
Blank Mild Steel	20.5	18.3	−164.1
Epoxy/PDG-g-PANI/Al ₂ O ₃ coated MS	72.7	70.3	−22.3

For a closer understanding of the thermodynamics behind the anti-corrosion coating, the change of formation enthalpy (ΔH_a^o) and entropy (ΔS_a^o) of the activation complex between metal surface and coating material in the transition state is given by the transition-state Equation (4) [36],

$$\log \frac{C_r}{T} = \log \left(\frac{R}{Nh} \right) + \frac{\Delta S_a^o}{2.303R} - \frac{\Delta H_a^o}{2.303RT} \tag{4}$$

where *N* is Avogadro’s number and *h* is Planck’s constant. A plot of $\log \frac{C_r}{T}$ over $1/T$, gives a straight line with the slope = $\frac{\Delta H_a^o}{2.303R}$ and intercept $\log \left(\frac{R}{Nh} \right) + \frac{\Delta S_a^o}{2.303R}$ from which the values of enthalpy and entropy were calculated (Figure 15a,b). The values of enthalpy and entropy are given in Table 9. The higher and positive values of enthalpy for coated MS compared to uncoated MS suggested that the corrosion/dissolution process is more difficult and endothermic in coated MS. Additionally, entropy of activation ΔS_a^o for coated MS is less negative, showing an ordered arrangement of particles present in the coating on the surface of MS. This confirms the activated complex as an association step rather than a dissociation step in the rate determining step [37]. From this study it is also concluded that the epoxy/composite coating thermodynamically inhibits the surface of steel from the corrosion process as well.

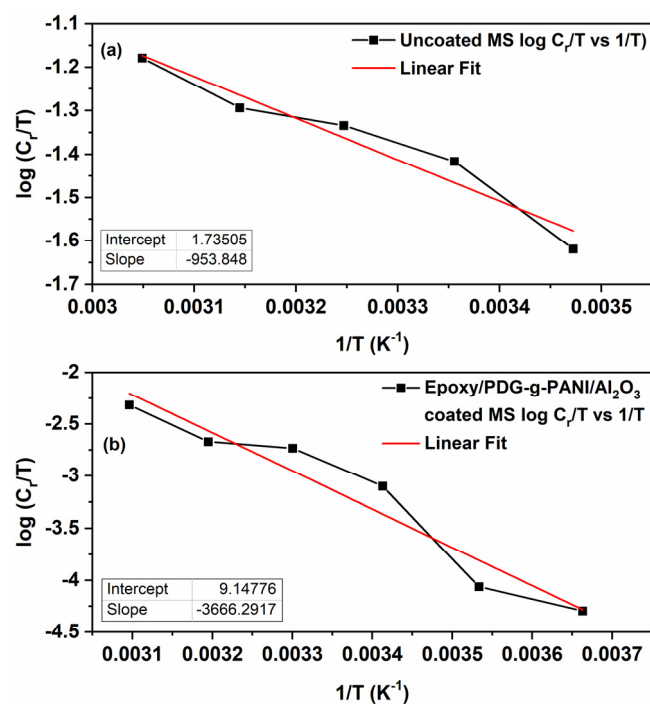


Figure 15. Extended Arrhenius plots of $\log C_r/T$ versus $1/T$ for (a) uncoated MS and (b) Epoxy/composite coated MS.

4. Conclusions

In this work, we successfully synthesized a green composite based on PDG-g-PANI/Al₂O₃ by a low-cost inverse emulsion polymerization. Material characterization showed that all three components were incorporated into a stable matrix, while cyclic voltammetry proved that the redox activity of PANI was preserved. The composite was used as an anti-corrosion coating for mild and stainless steel in salty and acidic media. The corrosion kinetic parameters obtained from the Tafel analysis showed that the PDG-g-PANI/Al₂O₃ composite protected the surface with a high inhibition efficiency of 92.3% and 51.9% for mild and stainless steel, respectively, in a 3.5% NaCl solution, which was significantly higher than the value without coating. When additionally dispersed in epoxy resin, the combination of epoxy and PDG-g-PANI/Al₂O₃ showed the best performance, with an inhibition efficiency of 99.9% for both steels in saline as well as acidic solution. Moreover, the anti-corrosion coating was maintained in a long-term study without significant changes in the inhibition efficiency. The analysis of Arrhenius plots for uncoated and coated mild steel showed that the corrosion process is strongly endothermic when the coating is applied, resulting in high stability. Overall, the high anti-corrosion efficiency can be attributed to (i) the excellent adhesion with outstanding mechanical strength of the epoxy resin, (ii) the adhesive behavior due to the presence of electron-rich functional groups and the good mechanical properties of PDG, and (iii) the redox reversibility of PANI.

Author Contributions: Conceptualization, M.K. and A.u.H.A.S.; methodology, M.K., G.R. and A.u.H.A.S.; formal analysis, M.K.; investigation, M.K. and G.R.; resources, A.u.H.A.S., S.B. and P.R.; data curation, M.K. and A.u.H.A.S.; writing—original draft preparation, M.K., A.u.H.A.S. and P.R.; writing—review and editing, A.u.H.A.S., S.B. and P.R.; visualization, M.K. and P.R.; supervision, A.u.H.A.S. and S.B.; project administration, A.u.H.A.S.; funding acquisition, A.u.H.A.S. and P.R. All authors have read and agreed to the published version of the manuscript.

Funding: The authors are thankful to Higher Education Commission Pakistan for providing funds for the establishment of Electrochemistry lab at the Institute of Chemical Sciences, University of Peshawar under NRPU project # 20-3111. The APC is funded by the KIT publication fund of Karlsruhe Institute of Technology, Germany.

Institutional Review Board Statement: Not applicable.

Informed Consent Statement: Not applicable.

Data Availability Statement: The data presented in this study are available on request from the corresponding author.

Conflicts of Interest: The authors declare no conflict of interest.

References

1. Pasha, A.; Khasim, S.; Darwish, A.A.A.; Hamdalla, T.A.; Al-Ghamdi, S.A. High Performance Organic Coatings of Polypyrrole Embedded with Manganese Iron Oxide Nanoparticles for Corrosion Protection of Conductive Copper Surface. *J. Inorg. Organomet. Polym. Mater.* **2022**, *32*, 499–512. [[CrossRef](#)]
2. Verma, C.; Olasunkanmi, L.O.; Akpan, E.D.; Quraishi, M.; Dagdag, O.; El Gouri, M.; Sherif, E.-S.M.; Ebenso, E.E. Epoxy resins as anticorrosive polymeric materials: A review. *React. Funct. Polym.* **2020**, *156*, 104741. [[CrossRef](#)]
3. Han, R.; He, H.; Liu, X.; Zhao, L.; Yang, Y.; Liu, C.; Zeng, R.-C. Anti-corrosion and self-healing coatings with polyaniline/epoxy copolymer-urea-formaldehyde microcapsules for rusty steel sheets. *J. Colloid Interface Sci.* **2022**, *616*, 605–617. [[CrossRef](#)] [[PubMed](#)]
4. Wang, W.; Wang, H.; Zhao, J.; Wang, X.; Xiong, C.; Song, L.; Ding, R.; Han, P.; Li, W. Self-healing performance and corrosion resistance of graphene oxide-mesoporous silicon layer-nanosphere structure coating under marine alternating hydrostatic pressure. *Chem. Eng. J.* **2019**, *361*, 792–804. [[CrossRef](#)]
5. Crespy, D.; Landfester, K.; Fickert, J.; Rohwerder, M. Self-healing for anticorrosion based on encapsulated healing agents. *Self-Heal. Mat.* **2016**, *273*, 219–245. [[CrossRef](#)]
6. Zotiadis, C.; Patrikalos, I.; Loukaidou, V.; Korres, D.M.; Karantonis, A.; Vouyiouka, S. Self-healing coatings based on poly(urea-formaldehyde) microcapsules: In situ polymerization, capsule properties and application. *Prog. Org. Coat.* **2021**, *161*, 106475. [[CrossRef](#)]

7. Thakur, T.; Gaur, B.; Singha, A. Bio-based epoxy/imidoamine encapsulated microcapsules and their application for high performance self-healing coatings. *Prog. Org. Coat.* **2021**, *159*, 106436. [[CrossRef](#)]
8. Tao, Z.; Cui, J.; Qiu, H.; Yang, J.; Gao, S.; Li, J. Microcapsule/silica dual-fillers for self-healing, self-reporting and corrosion protection properties of waterborne epoxy coatings. *Prog. Org. Coat.* **2021**, *159*, 106394. [[CrossRef](#)]
9. Li, J.; Shi, H.; Liu, F.; Han, E.-H. Self-healing epoxy coating based on tung oil-containing microcapsules for corrosion protection. *Prog. Org. Coat.* **2021**, *156*, 106236. [[CrossRef](#)]
10. Šobak, M.; Štular, D.; Štirn, Ž.; Žitko, G.; Čelan Korošič, N.; Jerman, I. Influence of the Prepolymer Type and Synthesis Parameters on Self-Healing Anticorrosion Properties of Composite Coatings Containing Isophorone Diisocyanate-Loaded Polyurethane Microcapsules. *Polymers* **2021**, *13*, 840. [[CrossRef](#)]
11. Shchukina, E.; Wang, H.; Shchukin, D.G. Nanocontainer-based self-healing coatings: Current progress and future perspectives. *Chem. Commun.* **2019**, *55*, 3859–3867. [[CrossRef](#)]
12. Ullah, H.; Qureshi, K.S.; Khan, U.; Zaffar, M.; Yang, Y.J.; Rabat, N.E.; Khan, M.I.; Saqib, S.; Mukhtar, A.; Ullah, S. Self-healing epoxy coating synthesis by embedment of metal 2-methyl imidazole and acetylacetonate complexes with microcapsules. *Chemosphere* **2021**, *285*, 131492. [[CrossRef](#)] [[PubMed](#)]
13. Wu, F.; Li, J.; Quan, H.; Han, J.; Liu, X.; Zhang, X.; Yang, J.; Xiang, Y. Robust polyurea/poly (urea–formaldehyde) hybrid microcapsules decorated with Al₂O₃ nano-shell for improved self-healing performance. *Appl. Surf. Sci.* **2021**, *542*, 148561. [[CrossRef](#)]
14. Ma, Y.; Liu, J.; Zhang, Y.; Ge, Y.; Wu, R.; Song, X.; Zhang, P.; Wu, J. Mechanical behavior and self-healing mechanism of polyurea-based double-walled microcapsule/epoxy composite films. *Prog. Org. Coat.* **2021**, *157*, 106283. [[CrossRef](#)]
15. Gupta, P.; Bajpai, M. Development of siliconized epoxy resins and their application as anticorrosive coatings. *Adv. Chem. Eng. Sci.* **2011**, *1*, 133–139. [[CrossRef](#)]
16. Yaqoob, A.A.; Serrà, A.; Bhawani, S.A.; Ibrahim, M.N.M.; Khan, A.; Alorfi, H.S.; Asiri, A.M.; Hussein, M.A.; Khan, I.; Umar, K. Utilizing Biomass-Based Graphene Oxide–Polyaniline–Ag Electrodes in Microbial Fuel Cells to Boost Energy Generation and Heavy Metal Removal. *Polymers* **2022**, *14*, 845. [[CrossRef](#)] [[PubMed](#)]
17. Birniwa, A.H.; Mahmud, H.N.M.E.; Abdullahi, S.S.; Habibu, S.; Jagaba, A.H.; Ibrahim, M.N.M.; Ahmad, A.; Alshammari, M.B.; Parveen, T.; Umar, K. Adsorption behavior of methylene blue cationic dye in aqueous solution using polypyrrole-polyethylenimine nano-adsorbent. *Polymers* **2022**, *14*, 3362. [[CrossRef](#)]
18. Sang, Y.; Liu, Q.; Wang, S.; Dong, S.; Fan, Y.; Zhao, X.; Li, S. Synthetic polyaniline-boron nitride-aqueous epoxy resin composite coating for improving the corrosion resistance of hot-dip galvanized steel plates. *Appl. Surf. Sci.* **2022**, *592*, 153229. [[CrossRef](#)]
19. Akbarinezhad, E.; Ebrahimi, M.; Faridi, H. Corrosion inhibition of steel in sodium chloride solution by undoped polyaniline epoxy blend coating. *Prog. Org. Coat.* **2009**, *64*, 361–364. [[CrossRef](#)]
20. Kamran, M.; Shah, A.A.; Rahman, G.; Bilal, S. Potential Impacts of Prunus domestica Based Natural Gum on Physicochemical Properties of Polyaniline for Corrosion Inhibition of Mild and Stainless Steel. *Polymers* **2022**, *14*, 3116. [[CrossRef](#)]
21. Peter, A.; Obot, I.B.; Sharma, S.K. Use of natural gums as green corrosion inhibitors: An overview. *Int. J. Ind. Chem.* **2015**, *6*, 153–164. [[CrossRef](#)]
22. Anjum, M.J.; Ali, H.; Khan, W.Q.; Zhao, J.; Yasin, G. Metal/metal oxide nanoparticles as corrosion inhibitors. *Corr. Prot. Nanoscale* **2020**, 181–201. [[CrossRef](#)]
23. Torknezhad, Y.; Khosravi, M.; Assefi, M. Corrosion protection performance of nanoparticle incorporated epoxy paint assessed by linear polarization and electrochemical impedance spectroscopy. *Corros. Mater.* **2018**, *69*, 472–480. [[CrossRef](#)]
24. Palaniappan, S.; Amarnath, C.A. A novel polyaniline–maleic acid–dodecylhydrogensulfate salt: Soluble polyaniline powder. *React. Funct. Polym.* **2006**, *66*, 1741–1748. [[CrossRef](#)]
25. Bilal, S.; Gul, S.; Holze, R.; Shah, A.A. An impressive emulsion polymerization route for the synthesis of highly soluble and conducting polyaniline salts. *Synth. Met.* **2015**, *206*, 131–144. [[CrossRef](#)]
26. Shah, A.A.; Kamran, M.; Bilal, S.; Ullah, R. Cost Effective Chemical Oxidative Synthesis of Soluble and Electroactive Polyaniline Salt and Its Application as Anticorrosive Agent for Steel. *Materials* **2019**, *12*, 1527. [[CrossRef](#)] [[PubMed](#)]
27. Ullah, R.; Yaseen, S.; Shah, A.A.; Bilal, S.; Kamran, M.; Rahim, M. Anticorrosive polyaniline synthesized using coconut oil as the dispersion medium. *Mater. Chem. Phys.* **2021**, *273*, 125071. [[CrossRef](#)]
28. Sanches, E.A.; de Souza, S.M.; Carvalho, A.P.L.; Trovati, G.; Fernandes, E.G.; Mascarenhas, Y.P. Nanocomposite based on polyaniline emeraldine-base and α -Al₂O₃: A structural characterization. *Int. J. Mater. Res.* **2015**, *106*, 1094–1100. [[CrossRef](#)]
29. Wang, F.; Ma, J.; He, G.; Chen, M.; Zhang, C.; He, H. Nanosize Effect of Al₂O₃ in Ag/Al₂O₃ Catalyst for the Selective Catalytic Oxidation of Ammonia. *ACS Catal.* **2018**, *8*, 2670–2682. [[CrossRef](#)]
30. Benykhlef, S.; Bekhoukh, A.; Berenguer, R.; Benyoucef, A.; Morallon, E. PANI-derived polymer/Al₂O₃ nanocomposites: Synthesis, characterization, and electrochemical studies. *Colloid Polym. Sci.* **2016**, *294*, 1877–1885. [[CrossRef](#)]
31. Bilal, S.; Gul, S.; Ali, K.; Shah, A.A. Synthesis and characterization of completely soluble and highly thermally stable PANI-DBSA salts. *Synth. Met.* **2012**, *162*, 2259–2266. [[CrossRef](#)]
32. Shabani-Nooshabadi, M.; Ghoreishi, S.; Jafari, Y. Electrosynthesis of polyaniline-TiO₂ nanocomposite films on aluminum alloy 3004 surface and its corrosion protection performance. *J. Nanostruct.* **2013**, *3*, 65–77. [[CrossRef](#)]
33. Rouhollahi, A.; Barzegar Khaleghi, M.H. Epoxy-based PANI/zinc oxide/glass fiber nanocomposite coating for corrosion protection of carbon steel. *Corros. Mater.* **2018**, *69*, 393–401. [[CrossRef](#)]

34. Tavandashti, N.P.; Almas, S.M.; Esmailzadeh, E. Corrosion protection performance of epoxy coating containing alumina/PANI nanoparticles doped with cerium nitrate inhibitor on Al-2024 substrates. *Prog. Org. Coat.* **2021**, *152*, 106133. [[CrossRef](#)]
35. Noor, E.A.; Al-Moubaraki, A.H. Thermodynamic study of metal corrosion and inhibitor adsorption processes in mild steel/1-methyl-4 [4'(-X)-styryl pyridinium iodides/hydrochloric acid systems. *Mater. Chem. Phys.* **2008**, *110*, 145–154. [[CrossRef](#)]
36. Udensi, S.; Ekpe, O.; Nnanna, L. New bouldia laevis leaves extract as tenable eco-friendly corrosion inhibitor for aluminium alloy AA7075-T7351 in 1 M HCL corrosive environment: Gravimetric, electrochemical and thermodynamic studies. *Chem. Afr.* **2020**, *3*, 303–316. [[CrossRef](#)]
37. Shivakumar, S.; Mohana, K. Studies on the inhibitive performance of Cinnamomum zeylanicum extracts on the corrosion of mild steel in hydrochloric acid and sulphuric acid media. *J. Mater. Environ. Sci.* **2013**, *4*, 448–459.